The 9th European Congress on Computational Methods in Applied Sciences and Engineering
ECCOMAS Congress 2024
3–7 June 2024, Lisboa, Portugal

NUMERICAL STUDY OF MAGNETOHYDRODYNAMIC HYPERSONIC FLOW AROUND A BLUNT BODY USING OPENFOAM

ODELMA S. TEIXEIRA[1] AND JOSÉ C. PÁSCOA[2]

[1,2] C-MAST Center for Mechanical and Aerospace Science and Technology
Universidade da Beira Interior, Departamento de Engenharia Eletromecânica,
6201-001, Covilhã, Portugal
e-mail[1]: odelma.teixeira@ubi.pt and e-mail[2]: pascoa@ubi.pt

Key words: Magnetohydrodynamic, Hypersonic Flow, Numerical Simulation, OpenFOAM

Summary.

In the present work, a high enthalpy hypersonic flow of Mach 17.1 and 14.9 MJ/kg of stagnation enthalpy, around a cylindrical blunt body is numerically studied using a density-based compressible algorithm in OpenFOAM. The flow field and surface properties for different magnetic field intensities and different electrical conductivity models were analysed and it was possible to conclude that the choice of the correct electrical conductivity model is of extreme importance to have an accurate prediction of the MHD flow control mechanism. With the present conditions, it was observed no significant change in the flow field and surface properties using the Chapman Cowling electrical conductivity model, even for magnetic field intensities as great as 2 T. While for the Bush model the flow field and surface properties clearly changed with the magnetic fields, resulting in an increase of the shock standoff distance and a reduction on surface pressure. It was found that the Lorentz force for the Bush model is hundreds of times higher than the Lorentz force obtained with the Chapman Cowling model and that it would be required to apply a magnetic field in the flow field near the body surface of 3.8 T to get the same Lorentz force with both conductivity models.

1 INTRODUCTION

The comprehension of hypersonic flight is becoming more and more important and serve as an accelerating mechanism to advance in space exploration. Hypersonic flows can be described as those flows where the Mach number attains significant values, generally exceeding Mach 5. Among other crucial phenomena, they are distinguished by very high temperatures, the interaction between the boundary layer and shock waves, molecular dissociation, vibrational excitation, species diffusion, and ionization processes [1, 2]. The extreme temperatures, typically generated due to the strong shock, established the numerical approach as the principal method to analyze hypersonic flows in a feasible and consistent manner. Numerical methods are essential for grasping the effects of relevant flow-field parameters, which would be rather difficult to explore through experimentation. For this aim, Computational Fluid Dynamics (CFD) and Direct Simulation Monte Carlo (DSMC) advanced computational techniques have been extensively used [3, 2, 4, 5].

Early studies in MHD applied to re-entry vehicles suggested that the ionized air in the shock layer, which electrical conductivity at the stagnation point and the surrounding regions can attain several hundred mho/m, will interact with the magnetic field at the vehicle's nose and alter the location of the bow shock and decrease the heat flux at the vehicle surface [6, 7, 8, 9, 10, 11, 12, 13, 14, 15]. More recently, there has been a revival of interest on plasma-assisted technology in high-speed flight, with applications including scramjet engine intake control, aerodynamic heating reduction, communication blackout mitigation, and aerobraking [16, 17, 18, 19, 20, 21, 22]. Although the capability of MHD flow control technologies has been demonstrated, its efficacy remains an unresolved issue, and more sophisticated numerical simulation tools are demanded in order to face the new challenges in the aerospace industry [23]. Various simulation software packages for hypersonic reacting flow, including DPLR, LAURA, LeMANS, US3D, OpenFOAM have been using. Different from the all other simulation software, OpenFOAM has the advantage of being open-source, flexible, with a robust class structure for numerical modeling and a wide community of contributions.

In the present work, the MHD effects on a hypersonic flow around a blunt body is numerically investigated considering different electrical conductivity models and a wide range of magnetic fields. A thermochemical non-equilibrium compressible flow code with 11-species air chemistry and two temperature model is here employed in the OpenFOAM framework in order to study the flow field around the blunt body.

2 MATHEMATICAL FORMULATION

2.1 Governing equations

The governing equations correspond to the full Navier-Stokes-Fourier resistive-MHD system with the low magnetic Reynold's number approximation. Since the flow around re-entry vehicles is low-ionized, the low magnetic Reynolds number's approximation is justified [24], and the governed equations are defined below:

$$\frac{\partial \mathbf{U}}{\partial t} + \frac{\partial (\mathbf{F}_{i,inv} - \mathbf{F}_{i,vis})}{\partial x_i} = \dot{\mathbf{S}} + \dot{\mathbf{S}}_{\mathbf{MHD}} \tag{1}$$

Where $\mathbf{U}$ is the vector of conserved quantities defined as,

$$\mathbf{U} = \{\rho, \rho_s, \rho u, \rho v, \rho w, E_{ve,m}, E_t\}^T \qquad s \in N_s, \quad m \in N_m \,. \tag{2}$$

where ρ and ρ_s being the total density of the fluid and the partial density of species s, respectively, u, v and w are the three components of the velocity vector and $E_{ve,m}$ and E_t are the total vibro-electronic energy of molecule m and the total energy, respectively.

The vectors $\mathbf{F}_{i,inv}$ and $\mathbf{F}_{i,vis}$ correspond to the inviscid and viscous flux vectors respectively.

The two source term vectors, $\dot{\mathbf{S}}$ and $\dot{\mathbf{S}}_{\mathbf{MHD}}$ correspond to the thermochemical and magneto-hydrodynamic source terms, respectively and are defined as:

$$\dot{\mathbf{S}} = \{0, \dot{w}_s, 0, 0, 0, \dot{w}_{v,m}, 0\}^T \tag{3}$$

The term $\dot{w}_s$ is the net mass production of species s due to the chemical reactions, here computed according to Park'93 reaction model [25]. $\dot{w}_{v,m}$ is the vibrational source term which is determined by the Landau-Teller equation [26] for vibrational-translational relaxation, using Millikan–White formula [27] and Park's correction [28] for the relaxation time.

The MHD source term vector, is defined by:

$$\dot{\mathbf{S}}_{\mathbf{MHD}} = \{0, 0, F_x, F_y, F_z, \mathbf{J} \cdot (\mathbf{u} \times \mathbf{B}), \mathbf{J} \cdot \mathbf{E} + \mathbf{u} \cdot \mathbf{F}\}^T \tag{4}$$

where F_x, F_y and F_z correspond to the three components of the Lorentz force vector, $\mathbf{F}$, with $\mathbf{F} = \mathbf{J} \times \mathbf{B}$, $\mathbf{J} \cdot (\mathbf{u} \times \mathbf{B})$ is the Joule heating generated by the induced electric current density, $\mathbf{J} \cdot \mathbf{E}$ is the Joule heating induced by the electric field, and $\mathbf{u} \cdot \mathbf{F}$ is the work done by the Lorentz force. Here $\mathbf{J}$, $\mathbf{E}$ and $\mathbf{B}$ correspond to the vector of the electric current density, the electric field vector and the magnetic field vector, respectively.

Hall and ion slip effects are neglected and the electrical current density is computed with the Ohm's law:

$$\mathbf{J} = \sigma(\mathbf{u} \times \mathbf{B}) \tag{5}$$

Two different models are used to compute the electrical conductivity. According to the Bush model [6], σ is expressed by:

$$\sigma = \sigma_{ref} \left(\frac{T_{tr}}{T_{ref}} \right)^n \tag{6}$$

where σ_{ref} and T_{ref} correspond to a reference electrical conductivity and a reference temperature, respectively, T_{tr} is the trans-rotational flow temperature, and n is the temperature exponent.

And, with the Chapman-Cowling model [29] the electrical conductivity is expressed as:

$$\sigma = 4.0229704 \times 10^{-18} \left(\frac{n_{e^-}}{\sqrt{T_{tr}}} \right) \tag{7}$$

where T_{tr} is the trans-rotational temperature, and n_{e^-} is the the electron number density.

2.2 Numerical methods

The computational code is an extension of that described in Ref. [30], with the addition of the MHD source terms. The governing equations are solved with the second-order central-upwind interpolation of Kurganov, Noelle and Petrova [23, 24]. Total variation diminishing (TVD) scheme with van Leer limiter function were used to compute the inviscid fluxes, and the second-order central difference scheme were used for the viscous fluxes [31, 32]. The time discretization was performed by using the first-order Euler scheme. The transport properties for each chemical species (N_2, O_2, NO, N, O, N_2^+, O_2^+, NO^+, N^+, O^+ and e^-) were computed using Blottner's and Eucken's formulae [33, 34]. The mixture properties were obtained by using the Armllly and Suton mixing rule [35].

3 DESCRIPTION OF THE TEST CASE

In this work, an axisymmetric cylindrical blunt body with a magnetic coil inside was used for the numerical study. Figure 1 (at left) shows the computational domain, with the grid and the boundary conditions. Five degree wedges were used to take advantage of the axysimmetry of the problem, allowing to reduce the computational cost keeping the numerical accuracy. The cylinder wall was considered to be fully catalytic, to be cooled, keeping at a fixed temperature

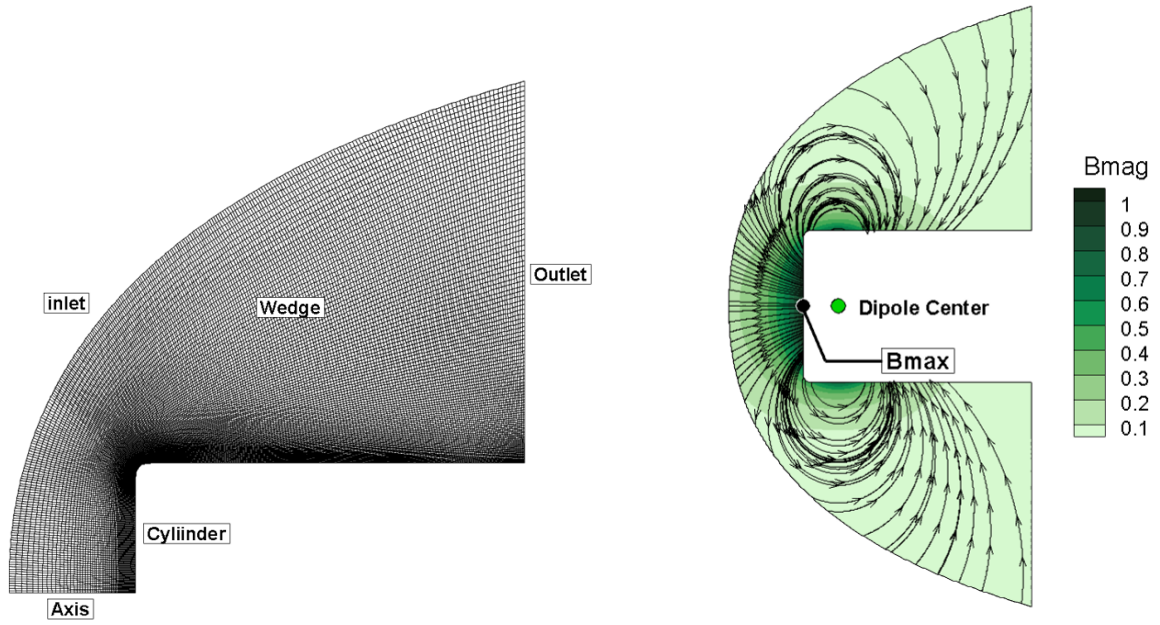

Figure 1: Computational domain (left) and magnetic field configuration (right)

Table 1: Freestream conditions.

U (m/s)	T_{tr} (K)	T_{ve} (K)	P (Pa)	Y_{N_2}	Y_{O_2}	Mach
5410	250	250	1300	0.7	0.3	17.1

of 300 K and to be electrically non-conductive. All the fields at the outlet are extrapolated from the domain.

The inlet conditions in terms of velocity (U), trans-rotational temperature (T_{tr}), vibro-electronic temperature (T_{ve}), pressure and mass fraction of molecular nitrogen and oxygen, Y_{N_2}, Y_{O_2}, and Mach number, are described in the Table 1. The Knudsen number is very small, about 5E-06, which confirm the contiunnum regime.

The dipole magnetic, Figure 1 (at right), is centered 75 cm from the cylindrical body frontal face, and its maximum value, Bmax, will be varying from 0 to 2 T.

4 RESULTS

In the present section, a presentation and discussion of the results is performed, starting with a grid independence analysis, following to the results obtained in the flow field, the results along the stagnation line and in the hypersonic body surface with different conductivity models.

4.1 Grid independence analysis

A estimation of the discretization error was perfomed by a grid convergence analysis, according to the Richardson extrapolation method [36, 37], using three different grid sizes, coarse, medium and fine, respectively, with clustering at the near wall regions for a good resolution of the boundary layer. Table 2 shows the grids used in the analysis with the corresponding number of cells and the grid spacing, h.

Table 2: Grid independence analysis

Grid size	No. of Cells	h (m)
Coarse	4042	0.021
Medium	10117	0.016
Fine	30302	0.011

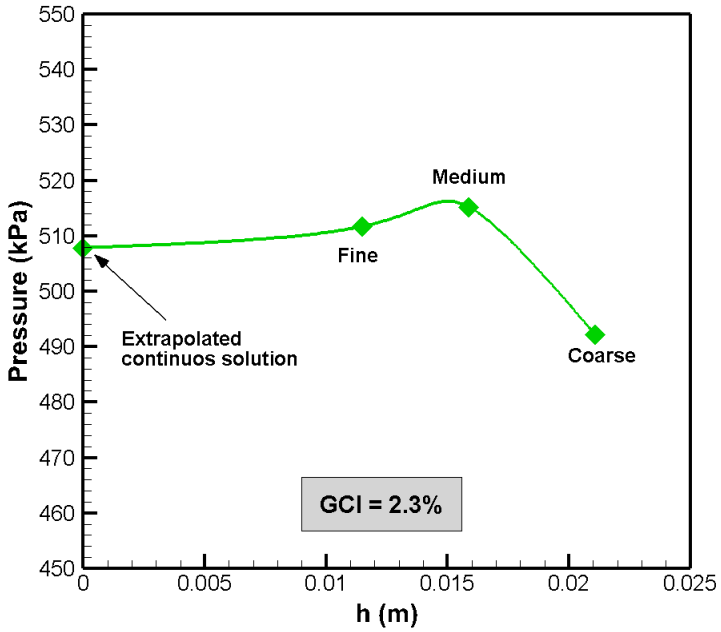

Figure 2: Grid convergence analysis: extrapolation of stagnation point pressure using the Richardson method and GCI.

Figure 2 shows the values of static pressure at the stagnation point, obtained using the three grids, and the extrapolated continuous solution, corresponding to a grid with infinitely small spacing, h. As it can be seen, the slope of the curve is close to zero as the grid spacing decreases, indicating a very good mesh quality for the Fine grid, with a static pressure value very close to the extrapolated continuous solution. The grid convergence index (CGI)[38], which is a measure of discretization uncertainty is of 2.3%. The Fine grid proved to give sufficiently accurate results and will be used in the subsequent analyses.

4.2 Impact on the flow field

Figure 3 shows the pressure distribution in the flow field around the studied body for different applied magnetic field intensities, for the Bush conductivity model. It is possible to see the shock layer enlargement as the magnetic field increases, confirming the predictions of past researches and the validity of the present numerical model. The shock layer starts with a thin zone in the frontal face of the longitudinal cylindrical body and keeps growing in frontal direction. One can

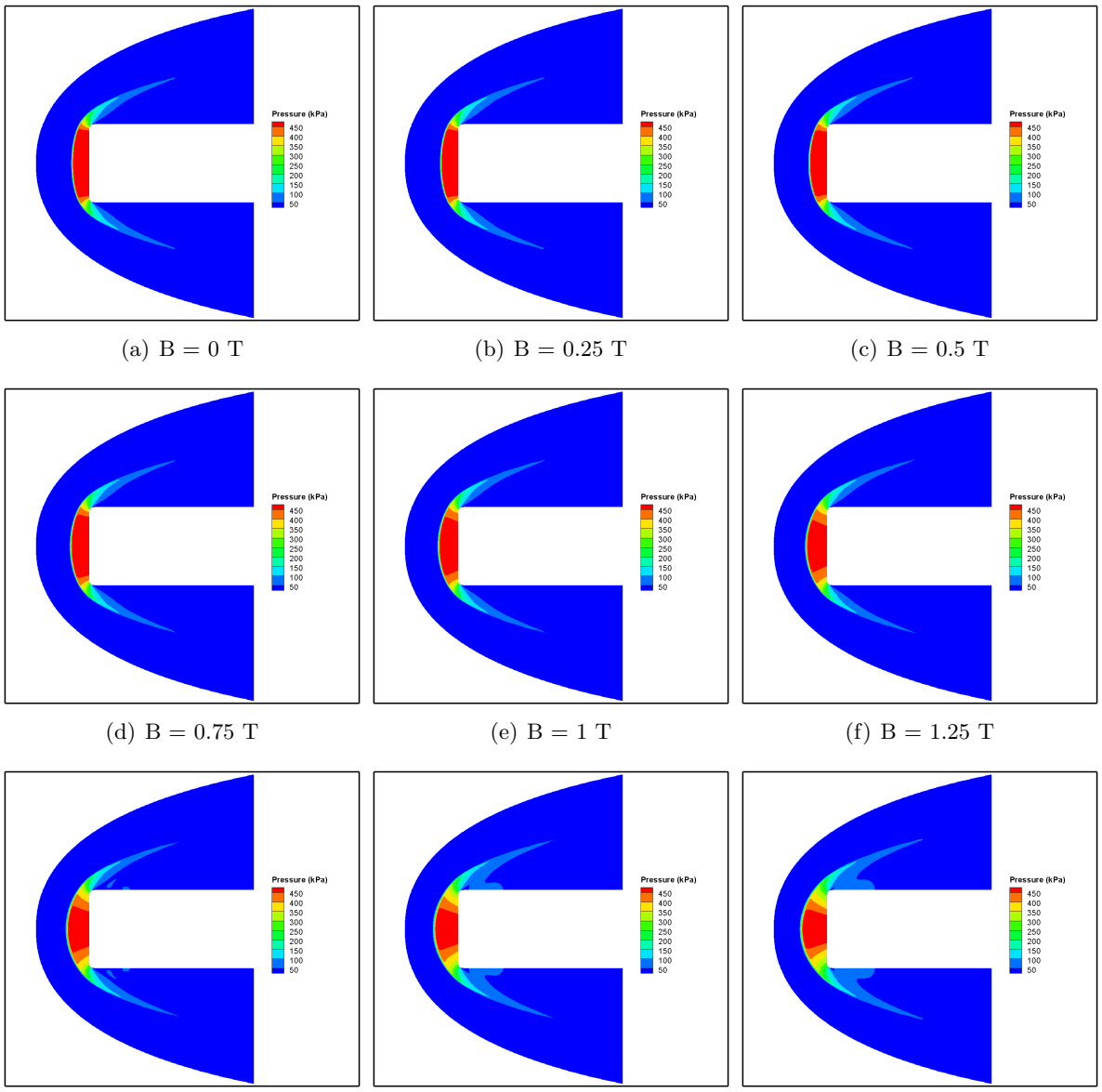

(a) B = 0 T (b) B = 0.25 T (c) B = 0.5 T

(d) B = 0.75 T (e) B = 1 T (f) B = 1.25 T

(g) B = 1.5 T (h) B = 1.75 T (i) B = 2 T

Figure 3: Pressure in the flow field for different magnetic field intensities for Bush conductivity model.

see more clearly that for a maximum magnetic field of B = 1.75 T and B = 2 T, Figures 3(h) and 3(i), respectively, the region near the lateral face of the cylindrical body is also affected by the magnetic field. Is is also possible to observe that the pressure in the flow field near the frontal face decreases in magnitude and in frontal area as the applied magnetic field increases.

Figure 4 shows the shock standoff distance as a function of the magnetic field intensity for Bush and Chapman Cowling electrical conductivity models. It is unquestionable the influence that the electrical conductivity model used in the numerical simulations can have in the MHD flow predictions. The shock standoff distances obtained with the Bush conductivity model

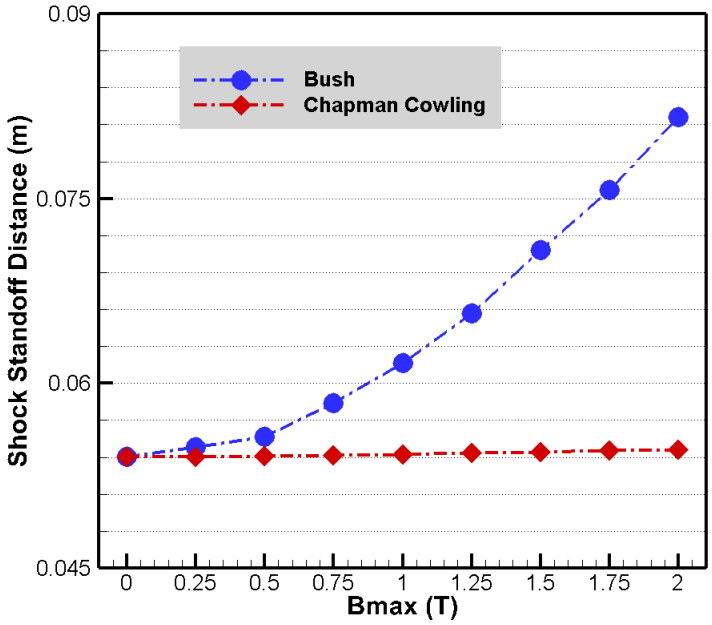

Figure 4: Standoff distance extension as a function of magnetic field intensity for different electrical conductivity models.

are much higher than the ones obtained with the Chapman Cowling model and its difference increases with increase of magnetic field intensity. We also found that the shock standoff distance growth with magnetic field has a polynomial distribution for the Bush model, while for the Chapman Cowling model the distribution is more likely linear.

Figure 5 represents the maximum Lorentz force obtained in the flow field with different magnetic field intensities for Bush and Chapman Cowling conductivity models. This results support the understanding of the previous results obtained for the shock-standoff distance. As it can bee seen, the Lorentz force for Bush conductivity model is hundreds of time higher than the Lorentz force obtained with the Chapman Cowling model. Further investigation here performed showed that the difference between the maximum Lorentz force obtained with both conductivity models decreases with the applied magnetic field, indicating that the at a certain magnetic field value they will be the same. In this case, it would be necessary to apply a maximum magnetic field in the flow field near the body surface of 3.8 T to get the same maximum Lorentz force with both conductivity models.

4.3 Impact at the stagnation line

The pressure distribution along the stagnation line (Y = 0) for the different electrical conductivity models is represented at Figure 6. One can see that at the studied conditions, corresponding to a Mach 17.1 flow with high stagnation enthapy of 14.9 MJ/kg, there was no significant change in the stagnation line pressure, when using the Chapman Cowling conductivity model, while for Bush model the pressure clearly changes with application of different values of magnetic

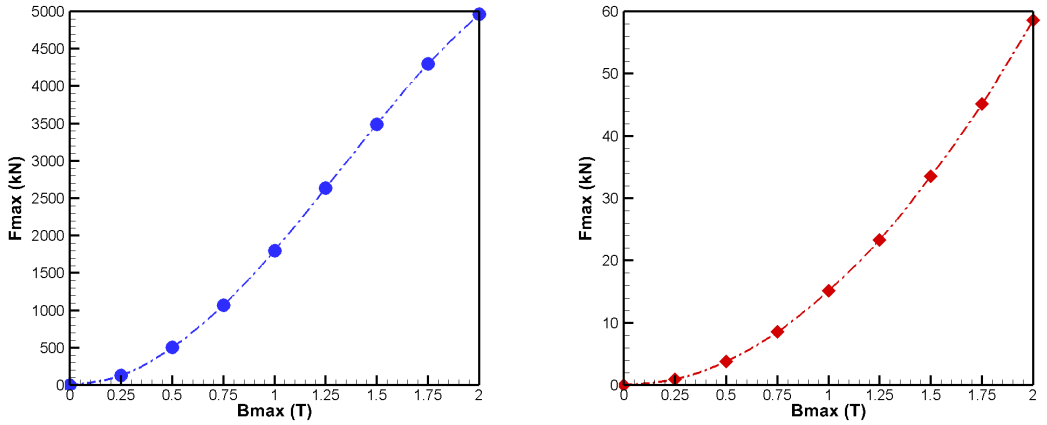

(a) Bush Conductivity Model (b) Chapman Cowling Conductivity Model

Figure 5: Lorentz force maximum value in the flow as a function of magnetic field intensity for different electrical conductivity models.

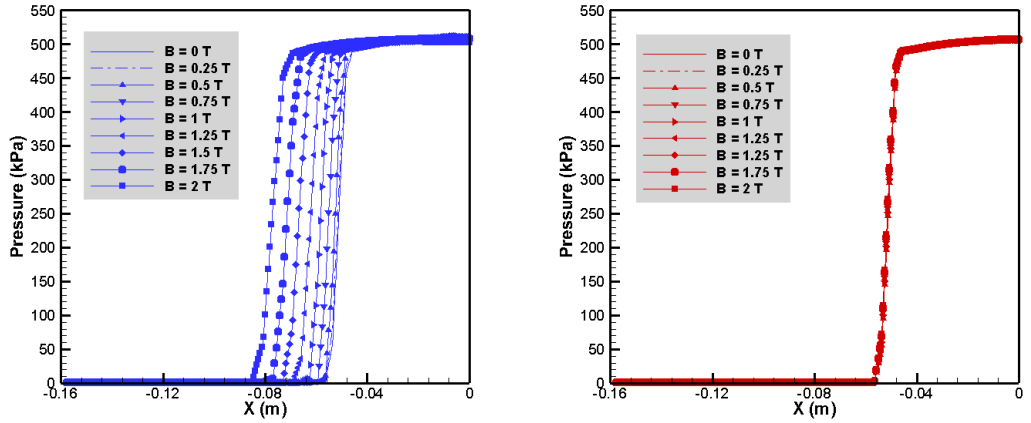

(a) Bush Conductivity Model (b) Chapman Cowling Conductivity Model

Figure 6: Pressure distribution at the stagnation line for different conductivity models.

field intensity, which was also seen in the shock standoff distance and shock-layer enlargement.

4.4 Impact at the blunt body surface

Figure 7 shows the pressure distribution along the cylindrical body surface for different magnetic field intensities and different conductivity models. The change in the pressure distribution in the flow field caused by the increase of the Lorentz force with the applied magnetic field in the Bush model is translated in a decrease on the pressure at the cylindrical body surface. This occurs because the increase of the shock standoff distance reduces the pressure gradient inside

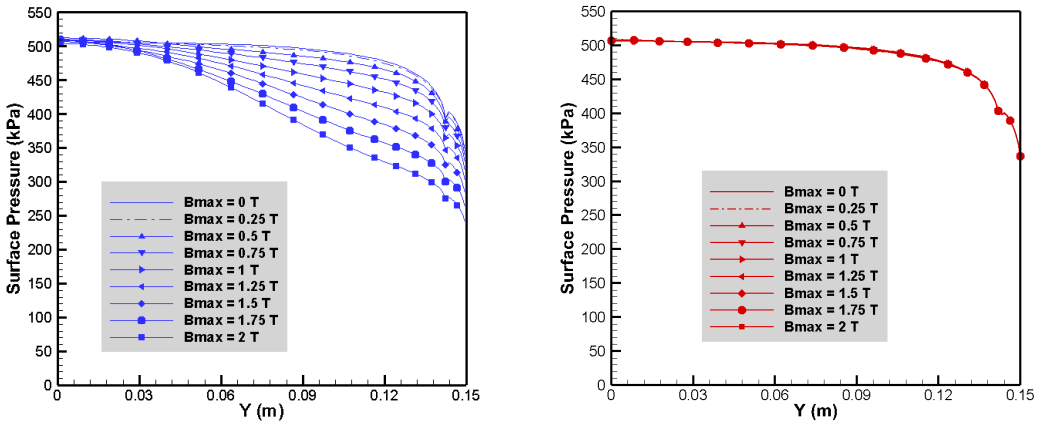

(a) Bush Conductivity Model (b) Chapman Cowling Conductivity Model

Figure 7: Pressure distribution along the cylindrical body surface for different conductivity models.

the shock-layer, reducing than the pressure at the hypersonic body surface. For the Chapman Cowling conductivity model, there was no meaningful change in the surface pressure by increasing the magnetic field intensity, a expected by the pressure distribution in the flow field and stagnation line.

5 CONCLUSIONS

The purpose of this work was to study numerically the MHD flow around a re-entry body in thermochemical non-equilibrium using different magnetic field intensities and different electrical conductivity models. Comparison between results with Bush and Chapman Cowling electrical conductivity models showed that the electrical conductivity models have a great influence on the MHD flow predictions. It was possible to observe that the shock standoff distances obtained with the Bush conductivity model are much higher than the values obtained by the Chapman Cowling models and that the difference between the two models results increases with the magnetic field intensity. The maximum Lorentz force in the flow field for the Bush model is hundreds of times higher than the Lorentz force obtained with the Chapman Cowling model. It was found that by applying a maximum magnetic field in the flow field near the cylindrical body surface of 3.8 T, it would be possible to obtain the same Lorentz force for both conductivity models. Due to the higher Lorentz force obtained with the Bush model, it was possible to decrease the surface pressure at the cylindrical body surface.

ACKNOWLEDGMENTS

The authors thank the Portuguese Foundation for Science and Technology, I.P. (FCT, I.P.) FCT/MCTES for the financial support with Grant No. UI/BD/153064/2022. This work was developed at the R& D Unit C-MAST/Center for Mechanical and Aerospace Science and Technologies with reference projects UIDB/00151/2020 (https://doi.org/10.54499/UIDB/00151/2020) and UIDP/00151/2020 (https://doi.org/10.54499/UIDP/00151/2020).

REFERENCES

[1] J. D. Anderson Jr., Hypersonic and High-Temperature Gas Dynamics, Second Edition, American Institute of Aeronautics and Astronautics, Reston,VA, 2006. doi:10.2514/4.861956.

[2] O. Teixeira, J. Pascoa, Hypersonic Flow Simulation towards Space Propulsion Geometries, SAE Int. J. Adv. Curr. Pract. Mobil. 2 (2) (2020) 803–810. doi:10.4271/2019-01-1873.

[3] O. Teixeira, J. Pascoa, Computational Modelling of Hypersonic Nozzles: The Influence of Enthalpy on the Flow Thermochemistry, in: AeroTech Conf. Exhib., SAE International, SAE Technical Paper No 2024-01-1935, Charlotte, North Caroline, USA, 2024. doi:10.4271/2024-01-1935.

[4] J.-J. O. Hoste, V. Casseau, M. Fossati, I. J. Taylor, R. Gollan, Numerical Modeling and Simulation of Supersonic Flows in Propulsion Systems by Open-Source Solvers, in: 21st AIAA Int. Sp. Planes Hypersonics Technol. Conf., American Institute of Aeronautics and Astronautics, Reston, Virginia, 2017. doi:10.2514/6.2017-2411.

[5] C. M. Xisto, J. C. Páscoa, P. J. Oliveira, A pressure-based high resolution numerical method for resistive MHD, J. Comput. Phys. 275 (2014) 323–345. doi:10.1016/j.jcp.2014.07.009.

[6] W. B. Bush, Magnetohydrodynamic-Hypersonic Flow Past a Blunt Body, J. Aerosp. Sci. 25 (11) (1958) 685–690. doi:10.2514/8.7845.

[7] E. L. Resler, W. R. Sears, The Prospects for Magneto-Aerodynamics, J. Aerosp. Sci. 25 (4) (1958) 235–245. doi:10.2514/8.7604.

[8] R. W. Ziemer, W. B. Bush, Magnetic Field Effects on Bow Shock Stand-Off Distance, Phys. Rev. Lett. 1 (2) (1958) 58–59. doi:10.1103/PhysRevLett.1.58.

[9] W. B. Ericson, A. Maciulaitis, Investigation of magnetohydrodynamic flight control, J. Spacecr. Rockets 1 (3) (1964) 283–289. doi:10.2514/3.27637.

[10] V. Bityurin, V. Zeigarnik, A. Kuranov, On a perspective of MHD technology in aerospace applications, in: 27th Plasma Dyn. Lasers Conf., American Institute of Aeronautics and Astronautics, Reston, Virigina, 1996. doi:10.2514/6.1996-2355.

[11] S. Kranc, R. W. Porter, A. B. Cambel, Electrodeless magnetogasdynamic power during entry., J. Spacecr. Rockets 4 (6) (1967) 813–815. doi:10.2514/3.28964.

[12] V.A. Bityurin, J.T. Lineberry, V.G. Potebnia, V.I. Alferov, A.L. Kuranov, E. Sheikin, Assessment of hypersonic MHD concepts, in: 28th Plasmadynamics Lasers Conf., American Institute of Aeronautics and Astronautics, Atlanta, Georgia, 1997.

[13] J. Lineberry, R. Rosa, V. Bityurin, A. Botcharov, V. Potebnya, Prospects of MHD flow control for hypersonics, in: 35th Intersoc. Energy Convers. Eng. Conf. Exhib., American Institute of Aeronautics and Astronautics, Reston, Virigina, 2000. doi:10.2514/6.2000-3057.

[14] J. Poggie, D. V. Gaitonde, Magnetic control of flow past a blunt body: Numerical validation and exploration, Phys. Fluids 14 (5) (2002) 1720–1731. doi:10.1063/1.1465424.

[15] V. Bityurin, A. Bocharov, J. Lineberry, MHD Flow Control in Hypersonic Flight, in: AIAA/CIRA 13th Int. Sp. Planes Hypersonics Syst. Technol. Conf., American Institute of Aeronautics and Astronautics, Reston, Virigina, 2005. doi:10.2514/6.2005-3225.

[16] A. Kulkarni, S. K. Yadav, A. Kumar, S. Ram, Recent advancements in scramjet engine: A review, 2023, p. 090019. doi:10.1063/5.0168817.

[17] Z. Wu, M. Ding, W. Dong, T. Gao, T. Jiang, Effect of MHD Control on Turbulent Boundary Layer Separation Flow in Scramjet Inlet, J. Phys. Conf. Ser. 2381 (1) (2022) 012015. doi:10.1088/1742-6596/2381/1/012015.

[18] Z. Zhou, Z. Zhang, Z. Gao, K. Xu, C.-H. Lee, Numerical Investigation on Mechanisms of MHD Heat Flux Mitigation in Hypersonic Flows, Aerospace 9 (10) (2022) 548. doi:10.3390/aerospace9100548.

[19] H. A. Muir, N. Nikiforakis, Numerical modeling of imposed magnetohydrodynamic effects in hypersonic flows, Phys. Fluids 34 (10) (oct 2022). doi:10.1063/5.0115424.

[20] J. S. Laur, V. F. Giangaspero, A. Lani, D. Luis, A. Viladegut, J. L. Gonzales Rios, J. Querol Borras, J. A. Vasquez-Peralvo, J. C. Merlano Duncan, A. Hein, J. Thoemel, Radio Communication Blackout Mitigation: A Three-Dimensional BlackOut RAy-Tracer (BORAT) with Signal Characterization for Magnetized Plasma, in: AIAA SCITECH 2024 Forum, American Institute of Aeronautics and Astronautics, Reston, Virginia, 2024. doi:10.2514/6.2024-1821.

[21] S. GUO, K. XIE, B. SUN, S. LIU, Mitigation of blackout problem for reentry vehicle in traveling magnetic field with induced current, Plasma Sci. Technol. 22 (12) (2020) 125301. doi:10.1088/2058-6272/abb455.

[22] D. E. Gildfind, D. Smith, A. Lefevre, P. A. Jacobs, T. J. McIntyre, Magnetohydrodynamic Aerobraking Shock Stand-Off Measurements with Flight Representative Electrodynamic Boundary Conditions, AIAA J. (2021) 1–15doi:10.2514/1.J060466.

[23] A. Ryakhovskiy, A. Schmidt, V. Antonov, Numerical Simulation of High-Speed Non-equilibrium Flow with Applied Magnetic Field, Proc. Inst. Syst. Program. RAS 29 (6) (2017) 299–310. doi:10.15514/ISPRAS-2017-29(6)-19.

[24] O. Khan, K. Hoffmann, J.-F. Dietiker, Validity of Low Magnetic Reynolds Number Formulation of Magnetofluiddynamics, in: 38th Plasmadynamics Lasers Conf., American Institute of Aeronautics and Astronautics, Reston, Virigina, 2007. doi:10.2514/6.2007-4374.

[25] C. Park, Review of chemical-kinetic problems of future NASA missions. I - Earth entries, J. Thermophys. Heat Transf. 7 (3) (1993) 385–398. doi:10.2514/3.431.

[26] L. Landau, E. Teller, ON THE THEORY OF SOUND DISPERSION, Phys. Zeitschrift der Sowjetunion 10 (34) (1936) 147–153. doi:10.1016/B978-0-08-010586-4.50027-4.

[27] R. C. Millikan, D. R. White, Systematics of Vibrational Relaxation, J. Chem. Phys. 39 (12) (1963) 3209–3213. doi:10.1063/1.1734182.

[28] C. Park, Nonequilibrium Hypersonic Aerothermodynamics, Wiley International, New York, 1990.

[29] S. Chapman, T. G. Cowling, The mathematical theory of non-uniform gases: an account of the kinetic theory of viscosity, thermal conduction and diffusion in gases, Cambridge University Press, 1970.

[30] O. Teixeira, J. Páscoa, Catalytic wall effects for hypersonic nozzle flow in thermochemical non-equilibrium, Acta Astronaut. 203 (2023) 48–59. doi:10.1016/j.actaastro.2022.11.031.

[31] C. J. Greenshields, H. G. Weller, L. Gasparini, J. M. Reese, Implementation of semi-discrete, non-staggered central schemes in a colocated, polyhedral, finite volume framework, for high-speed viscous flows, Int. J. Numer. Methods Fluids 63 (1) (2010) 1–21. doi:10.1002/fld.

[32] A. Kurganov, S. Noelle, G. Petrova, Semidiscrete Central-Upwind Schemes for Hyperbolic Conservation Laws and Hamilton–Jacobi Equations, SIAM J. Sci. Comput. 23 (3) (2001) 707–740. doi:10.1137/S1064827500373413.

[33] F. Blottner, M. Johnson, M. Ellis, Chemically Reacting Viscous Flow Program for Multi-Component Gas Mixtures., Tech. rep., Sandia National Laboratories (SNL), Albuquerque, NM, and Livermore, CA (United States) (jan 1971). doi:10.2172/4658539.

[34] V. Casseau, An Open-Source CFD Solver for Planetary Entry, Ph.D. thesis, University of Strathclyde (2017).

[35] B. Armaly, K. Sutton, Viscosity of multicomponent partially ionized gas mixtures, in: 15th Thermophys. Conf., American Institute of Aeronautics and Astronautics, Reston, Virigina, 1980. doi:10.2514/6.1980-1495.

[36] L. F. Richardson, J. A. Gaunt, VIII. The deferred approach to the limit, Philos. Trans. R. Soc. London. Ser. A, Contain. Pap. a Math. or Phys. Character 226 (636-646) (1927) 299–361. doi:10.1098/rsta.1927.0008.

[37] A. Meana-Fernández, J. M. Fernández Oro, K. M. Argüelles Díaz, M. Galdo-Vega, S. Velarde-Suárez, Application of Richardson extrapolation method to the CFD simulation of vertical-axis wind turbines and analysis of the flow field, Eng. Appl. Comput. Fluid Mech. 13 (1) (2019) 359–376. doi:10.1080/19942060.2019.1596160.

[38] P. J. Roache, Verification and validation in computational science and engineering, Albuquerque (N.M.) : Hermosa, 1998.